Antiviral drug discovery by targeting the SARS-CoV-2 polyprotein processing by inhibition of the main protease

Mahmoud Kandeel[1,2], Jinsoo Kim[3], Mahmoud Fayez[4,5], Yukio Kitade[6] and Hyung-Joo Kwon[3]

[1] Department of Biomedical Sciences, College of Veterinary Medicine, King Faisal University, Al-hofuf, Al-ahsa, Saudi Arabia
[2] Department of Pharmacology, Faculty of Veterinary Medicine, Kafrelshikh University, Kafrelshikh, Egypt
[3] Department of Microbiology, College of Medicine, Hallym University, Chuncheon, South Korea
[4] Al-Ahsa Veterinary Diagnostic Laboratory, Ministry of Agriculture, Al-Ahsa, Saudi Arabia
[5] Veterinary Serum and Vaccine Institute, Cairo, Dokki, Egypt
[6] Department of Applied Chemistry, Faculty of Engineering, Aichi Institute of Technology, Toyota, Japan

ABSTRACT

The spread of SARS-CoV-2, the causative agent for COVID-19, has led to a global and deadly pandemic. To date, few drugs have been approved for treating SARS-CoV-2 infections. In this study, a structure-based approach was adopted using the SARS-CoV-2 main protease (M^{pro}) and a carefully selected dataset of 37,060 compounds comprising M^{pro} and antiviral protein-specific libraries. The compounds passed two-step docking filtration, starting with standard precision (SP) followed by extra precision (XP) runs. Fourteen compounds with the highest XP docking scores were examined by 20 ns molecular dynamics simulations (MDs). Based on backbone route mean square deviations (RMSD) and molecular mechanics/generalized Born surface area (MM/G-BSA) binding energy, four drugs were selected for comprehensive MDs analysis at 100 ns. Results indicated that birinapant, atazanavir, and ritonavir potently bound and stabilized SARS-CoV-2 M^{pro} structure. Binding energies higher than -102 kcal/mol, RMSD values <0.22 nm, formation of several hydrogen bonds with M^{pro}, favourable electrostatic contributions, and low radii of gyration were among the estimated factors contributing to the strength of the binding of these three compounds with M^{pro}. The top two compounds, atazanavir and birinapant, were tested for their ability to prevent SARS-CoV-2 plaque formation. At 10 µM of birinapant concentration, antiviral tests against SARS-CoV-2 demonstrated a 37% reduction of virus multiplication. Antiviral assays demonstrated that birinapant has high anti-SARS-CoV-2 activity in the low micromolar range, with an IC50 value of 18 ± 3.6 µM. Therefore, birinapant is a candidate for further investigation to determine whether it is a feasible therapy option.

INTRODUCTION

The recent outbreak of SARS-CoV-2 has been declared a pandemic by WHO (*Cucinotta & Vanelli, 2020*). The disease COVID-19 causes a range of symptoms, from mild respiratory symptoms to severe respiratory distress associated with sepsis, multi-organ dysfunction, and

death (*Zaim et al., 2020*). The current alarming situation necessitates the rapid reallocation or repurposing of previously known drugs or chemical compounds for the use in treating COVID-19.

Approximately seven human coronaviruses (HCoV) have been identified. Four CoVs were identified as causative agents for mild respiratory symptoms and the common cold, including HCoV-229E, HCoV-NL63, HCoV-OC43, and HCoV-HKU1 (*Zeng et al., 2018*). However, more recently, severe symptoms and fatal outcomes have been caused by three other epidemic viruses, including SARS-CoV, MERS-CoV, and SARS-CoV-2. Coronaviruses express their nonstructural protein in the form of a large protein called polyprotein AB. This polyprotein has to be processed by the host as well as the viral encoded proteases to release approximately 16 NSPs. Two viral proteases share in the digestion of polyprotein AB: the main protease, called 3-C-like protease (M^{pro}), and a papain-like protease (PL^{pro}) (*Hilgenfeld, 2014*). Both PL^{pro} and M^{pro} have been important targets for drug discovery against SARS CoV, MERS CoV, and SARS CoV-2 (*Kandeel, Altaher & Alnazawi, 2019*; *Li et al., 2019*; *Pillaiyar, Meenakshisundaram & Manickam, 2020*; *Zumla et al., 2016*).

The magic bullet for treating SARS-CoV2 is drug repurposing. As a result, numerous compounds were developed as anti-SARS-CoV-2 agents and therapies or prevent the virus's sequelae, have been studied *in silico*, *in vitro*, and in human clinical trials (*Ghareeb et al., 2021*). Several molecular targets were utilized to develop novel chemicals to combat Coronaviruses such as virus spike (*Choudhary et al., 2021*), main protease (*Mostafa et al., 2021*), papain-like protease (*Delre et al., 2020*; *Mahmoud et al., 2021*), helicase (*Gurung, 2020*) and RNA-dependent RNA polymerase (*Molavi et al., 2021*).

In silico drug development investigations focused on the primary protease of SARS-CoV-2. The studies include docking and virtual screening of phytochemicals (*Mandal, Jha & Hazra, 2021*), Hepatic C virus FDA approved drugs (*Uddin et al., 2021*), clinically approved and investigational drugs (*Durdagi et al., 2021*), nonsteroidal anti-inflammatory drugs (*Abo Elmaaty et al., 2021*) and antiallergic agents (*Uras et al., 2021*). A combination of *in silico* and *in vitro* drug repurposing against the SARS-CoV-2 main protease resulted in the identification of several hopeful peptidomimetics (*Zhang et al., 2020*) and small molecules as diclazuril (*Pohl et al., 2021*), nilotinib (*Banerjee et al., 2021*), ritonavir, rotigaptide, and cefotiam (*Durdagi et al., 2021*).

Recently, we provided computational details regarding targeting the M^{pro} and PL^{pro}, wherein we used a dataset of FDA-approved drugs (*Kandeel et al., 2020*; *Kandeel & Al-Nazawi, 2020*). In this study, we used a more comprehensive virus-specific and M^{pro}-specific dataset of compounds. The selected compounds in this study (Table 1) were selected from chemical libraries of millions of compounds. The compounds were approved by chemical screening compounds libraries providers with the specific aims of (1) conducting a ligand and structure-based search of HTS databases using M^{pro} specific features, (2) performing a 2D fingerprint similarity search against the biologically active compounds from therapeutically relevant viral assays, and (3) exploring specific viral protein binding compounds, antiviral nucleotides, and nucleotide mimetics agents. A total of 37,060 compounds were retrieved and used in our virtual screening, docking, and

Table 1 The compounds dataset used in this study.

Library name	Company	Number of compounds	Method of selection
Main protease targeted library	Life chemicals (Niagara-on-the-Lake ON, Canada)	2,300	Glide by Schrödinger, SP mode was used to search Life chemicals HTS collection, by using the main protease of SARS-CoV-2 in complex with an inhibitor N3.
Antiviral Library by 2D Similarity	Life chemicals	19,244	Antiviral Screening Compounds Library was designed with 2D fingerprint similarity search against the 41,514 biologically active compounds from therapeutically relevant viral assays from different virus species.
Antiviral Library by Combined Ligand-based and Structure-based Approaches	Life chemicals	3,500	Antiviral protein targets were collected from the RCSB PDB. The reference antivirals were collected from ChEMBLdb and clustered according to the target. The top compounds were docked into the target protein and ranked.
Antiviral library	Asinex (Winston-Salem, NC USA)	6,827	Small molecules and macrocycles with antiviral activity. Specific designs include a-helix mimetics, glycomimetic, diverse synthetic macrocycles, and tri/tetra-substituted scaffolds.
Enamine antiviral library	Enamine (Monmouth Jct., NJ, USA)	4,842	Nucleoside-like antiviral agents or Nucleoside mimetics from screening collection. The compounds contain natural-like moieties and diverse heterocycles as bioisosters of nucleosides.
Antiviral compound library	Selleck (Houston, Texas, United States)	347	Collection of antiviral compounds
Total no. of compounds		37,060	

molecular dynamics simulations. The results will help in the design and application of new compounds in treating COVID-19.

MATERIALS AND METHODS

Construction of drugs and compounds dataset and ligand preparation

A total of 37,060 compounds dataset was constructed comprising SARS-CoV-2 main protease targeted library, compounds obtained from 2D fingerprint from therapeutically relevant antiviral assays, combined ligand and structure-based approaches of inhibitors of viral proteins (Table 1). All compounds were prepared for virtual screening by Ligprep software using OPLS2005 force field (Files S1 and S2).

SARS-CoV-2 M^{pro} protein preparation

The structure of M^{pro} (PDB ID 6lu7) was downloaded from the Protein Data Bank. The protein structure was processed and optimized using the Maestro software package's protein preparation wizard (Schrodinger LLC, NY, USA). The protein was protonated, the structure was optimized at cellular pH settings, and the structural energy was minimized using the OPLS2005 force field. The prepared structure was used in all docking and molecular dynamics calculations in this study.

Virtual screening

Docking of all compounds was performed by Schrodinger Glide docking module. Two-step docking runs were carried out. Initially, the compounds were docked by the standard precision docking protocol (SP docking). Compounds with docking scores of −8.00 or lower were retrieved and subjected to extra precision (XP-docking). This score is suggested to be strong binding compounds with shallow or hydrophobic cavities. The co-crystallized ligand served as the core of a 20-size docking box that encircled the bound ligand in the creation of the docking grid. The obtained results were ranked according to the obtained docking scores.

Molecular dynamics (MD) simulations

The MD simulations were carried out using GROMACS 5.1.4. (*Abraham et al., 2015*; *Van Der Spoel et al., 2005*). The parameters and optimization of the simulation system were as previously reported (*Al-Hizab & Kandeel, 2021*). Briefly, protein and ligands were handled by AMBERFF14SB and AMBER force field (GAFF). The complexes were dissolved in a single point charge water model in a cubic box of 1.0 nm. For 5000 steps, the solvated M^{pro}-ligand complexes were minimized. At 300K, the entire system was equilibrated in two phases: NVT ensemble of 50 ps, followed by NPT ensemble for 1 ns. For all compounds, the production stages were extended to 20 ns. The simulations of the top four compounds were then extended to 100 ns. The pressure and temperature contrls were by Parrinello-Rahman algorithm and V-rescale thermostat algorithm, respectiely. For long-range electrostatics, the Particle Mesh Ewald (PME) technique was utilized (12 Å direct space cut-off). A two fs was chosen as the time step. The output data were collected every 10 ps. In the trajectory analysis, GROMACS MD simulation toolkits were used. The root mean square deviation (RMSD) and per-residue root mean square fluctuation (RMSF) of protein residues were calculated using the g rms and g rmsf functions, respectively. The binding energy was calculated using the g mmpbsa tool (*Kumari et al., 2014*).

SARS-CoV-2 plaques inhibition assay
Cell line and virus

African green monkey kidney Vero E6 cells were purchased from the Korean Cell Line Bank (Seoul, Korea). The incubation and handling of cells was as previously described (*Kandeel et al., 2021*). The Korean Cell Line Bank authenticated Vero E6 cells with tests for morphology, growth pattern, histopathology, DNA fingerprinting, and mycoplasma contamination. We also checked the mycoplasma contamination using mycoplasma PCR detection kit (Myco-sniff^{TM} mycoplasma PCR detection kit; MP Biomedicals, Irvine, CA, USA). We prepared stocks for the cell line at early passages, and the cell line was maintained until passage 20 (within 2 months) and then discarded. SARS-CoV-2 S clade (hCoV-19/South Korea/KCDC03/2020, EPI_ISL_407193) was provided by the National Culture Collection for Pathogens (Osong, Korea).

Virus amplification and virus quantification by plaque assay

Vero E6 cells (5×10^4 cells/well 6-well plates) were cultured overnight. The cells were infected with SARS-CoV-2 in PBS (0.1 MOI) for 1 h in a CO_2 incubator at 37 °C, then

2 ml of DMEM containing 2% FBS was added. After 3 h incubation in a CO_2 incubator at 37 °C, the cells were treated with DMSO (0.1%), birinapant (10 μM) or atazanavir (10 μM) and incubated for 48 h. The virus replication was evaluated using the plaque formation assay. SARS-CoV-2 experiments were approved by the Institutional Biosafety Committee of Hallym University (Permit no. Hallym2020-12) and The amplification of SARS-CoV-2 and the experimental techniques were carried out under a biosafety level 3 (BSL-3) environment.

Statistical analysis

Correlation statistics were carried out by GraphPad Prism software. Pearson's correlation coefficient was used to conclude the significance of the results.

RESULTS

Virtual screening and docking

Recently, we used molecular modeling, virtual screening, and MD) simulation in characterization of the biological aspects of microbial agents, characterization of diseases, and drug discovery (*Altaher & Kandeel, 2016*; *Altaher, Nakanishi & Kandeel, 2015*; *Sheikh et al., 2020*). This study used an antiviral and M^{pro}-specific dataset. Virtual screening and docking comprised a two-step process. First, an initial standard-precision (SP) docking protocol was performed, with compounds having a docking score of −8.00 or higher (453 compounds) selected for extra-precision (XP) evaluation. File S1 contains the docked compounds ordered by docking score. After SP-docking, the selected compounds were exported in SDF format and redocked using the XP-docking module, the results of which are provided in File S2. The top 14 compounds with the highest docking scores were used in MD simulations, taking lopinavir as a reference inhibitor (Table 2). All of the top compounds showed favourable profiles and negative scores for Hbond, hydrophobic interactions, vdw, and coulombic interactions. Likewise, the calculated binding energy scores (MM-GBSA) were favourable and indicated strong binding profiles, with values ranging from −56.67 to −106.64 kcal/mol (Table 1).

Statistical analysis comprised determining the correlation between the obtained docking score and ligand efficiency, lipo, Hbond, vdw, coulombic, Glide energy, and binding energy scores (Table 3). A strong negative correlation was observed between docking score and lipophilic interactions ($r = -0.60$, $p > 0.05$), and a positive correlation with columbic interactions ($r = 0.74$, $p > 0.05$). This implies a predominance of electrostatic interactions in compounds binding with SARS-CoV-2 M^{pro}.

The determined binding features for each compound with M^{pro} are provided in Fig. 1. The binding site is mostly composed of hydrophobic residues (THR24, THR25, LEU27, VAL42, MET49, PRO52, TYR54, PHE140, LEU141, MET165, LEU167, and THR190); also present are few positively charged residues (ARG188), negatively charged residues (GLU166 and ASP187), and neutral residues (CYS44, SER144, GLN189, and GLN192).

Molecular dynamics simulations for 20 ns

A potent drug discovery tool is the combination of docking and MD modelling. Drugs can be graded based on their binding affinity and precise interaction with ligand–receptor

Table 2 Virtual screening and docking output of the top fourteen compounds.

Title	Docking score	Glide ligand efficiency	Glide lipo	Glide hbond	Glide evdw	Glide ecoul	Glide energy	MMGBSA _dG_Bind
Rutin	−11.78	−0.27	−2.62	−0.16	−47.64	−27.84	−75.49	−88.91
(-)-Epigallocatechin	−11.57	−0.35	−2.91	−0.65	−34.90	−24.05	−58.95	−70.18
Sennoside A	−10.77	−0.17	−2.13	−0.14	−39.11	−18.62	−57.73	−61.40
asinex8472	−9.83	−0.32	−2.83	−1.23	−38.99	−11.59	−50.58	−64.51
Atazanavir	−9.81	−0.34	−3.11	−1.28	−37.43	−13.69	−51.11	−74.66
asinex8485	−9.78	−0.33	−2.69	−1.33	−42.63	−11.63	−54.25	−73.40
asinex6886	−9.71	−0.30	−3.50	−0.84	−45.42	−8.69	−54.11	−56.67
Alpha-Mangostin	−9.14	−0.31	−3.68	−0.83	−42.12	−8.79	−50.91	−93.46
Glycitin	−8.83	−0.28	−2.96	−0.32	−32.44	−15.39	−47.83	−77.38
Birinapant	−8.81	−0.15	−3.67	−0.46	−60.32	−14.06	−74.38	−106.64
F2583-0433	−8.80	−0.29	−2.97	−1.20	−42.87	−17.08	−59.95	−89.30
F3234-0818	−8.65	−0.30	−3.03	−0.90	−43.91	−12.30	−56.20	−72.79
Lopinavir	−8.68	−0.15	−4.90	−0.16	−61.64	−7.72	−69.36	−84.25
Cobicistat	−8.55	−0.10	−4.48	−0.26	−54.69	−14.25	−68.94	−82.33

intermediates using these methods. MD simulation and post-dynamic binding energy analysis were performed on the top-ranked compounds from XP-docking. Two stages of compound filtering were used. The RMSD, RMSF, and binding energy values of all 14 compounds were calculated after they were simulated in MD for 20 ns. The top four compounds were studied in a more extensive 100 ns simulation in the second stage. The structural changes in M^{pro} backbone residues were compared (Fig. 2). All treatment complexes, with the exception of Apo M^{pro} and M^{pro} combined with cobicistat and glycitin, showed high stability.

MM-GBSA binding energies

The MM-GBSA binding energies of the 14 compounds ranged from −42.627 kcal/mol to −42.627 kcal/mol. The top six compounds showed MM-GBSA binding energies ranging from −102.564 to −139.154, indicating a likely substantial binding affinity. Furthermore, all of the investigated compounds had low structural RMSD throughout the 20 ns simulations, with RMSD values as low as 0.21 nm (Table 4).

Molecular dynamics simulations for 100 ns

To gain a better understanding of the strongest-binding drugs, the four drugs with binding energies greater than −100 kcal/mol (alpha-mangostin, atazanavir, birinapant, and lopinavir) were subjected to 100 ns MD simulations, followed by analyses of RMSD, RMSF, hbond length, and Rg and binding energy. All four had promising binding free energy values (Table 4). Specifically, the estimated MM-GBSA binding energy values were −117.90, −117.83, −121.80, and −112.80 for alpha-mangostin, atazanavir, birinapant, and lopinavir, respectively. The three drugs alpha-mangostin, atazanavir, and birinapant are implied by these values to have superior binding over lopinavir.

Table 3 Correlation statistics of the obtained docking score and the output parameters of XP-docking.

	Docking score *vs.* glide ligand efficiency	Docking score *vs.* glide lipo	Docking score *vs.* glide hbond	Docking score *vs.* glide evdw	Docking score *vs.* glide ecoul	Docking score *vs.* glide energy	Docking score *vs.* MMGBSA_dG_Bind
Pearson r							
r	0.3446	−0.6011	−0.1216	−0.3886	0.741	0.08881	−0.3251
95% confidence interval	−0.2275 to 0.7399	−0.858 to −0.1035	−0.6127 to 0.4371	−0.7621 to 0.1788	0.3468 to 0.9127	−0.4636 to 0.5915	−0.7298 to 0.2483
R squared	0.1188	0.3613	0.0148	0.151	0.5491	0.007888	0.1057
***P* value**							
P (two-tailed)	0.2275	0.0230	0.6787	0.1697	0.0024	0.7627	0.2567
P value summary	ns	*	ns	ns	**	ns	ns
Significant? (alpha = 0.05)	No	Yes	No	No	Yes	No	No
Number of XY Pairs	14	14	14	14	14	14	14

Figure 1 The docking site and ligands interactions with M^pro^. (A) The docking site of M^pro^ following XP docking protocol. (B) Surface representation (blue) of birinapant in the active site of M^pro^. (C) The binding site of residues of atazanavir. (D) The binding site residues of birinapant. (E) The ligand interactions of atazanavir. (F) The ligand interactions of birinapant. Hydrogen bonds are shown in purple arrows, hydrophobic interactions in grey circles.

Full-size 🖼 DOI: 10.7717/peerj.12929/fig-1

Figure 2 (A–C) **RMSD plot of the top fourteen compounds after MDS for 20 ns.** Lopinavir was used for reference. Apo structure is M^{pro} without any ligands.

Full-size ⬜ DOI: 10.7717/peerj.12929/fig-2

Table 4 The MM-GBSA binding energy and the average structure RMSD of the top fourteen compounds after MDS for 20 ns.

Compound ID	Binding energy (kcal/mol)	Average structure RMSD (nm)
Birinapant	−139.154	0.171
Atazanavir	−130.299	0.180
Lopinavir	−114.654	0.138
Cobicistat	−111.296	0.214
Alpha-Mangostin	−107.446	0.151
8472	−102.564	0.151
(-)-Epigallocatechin gallate	−88.348	0.155
3754	−83.21	0.160
3234–0818	−77.978	0.157
2583–0433	−73.954	0.201
8458	−70.288	0.165
6886	−70.18	0.171
Rutin	−47.388	0.169
Glycitin	−42.627	0.175
Sennoside A	59.744	0.138

After 100 ns MDs, average RMSD values of 0.23, 0.20, 0.21, and 0.18 nm were obtained for alpha-mangostin, atazanavir, birinapant, and lopinavir, respectively. Relative to experimental RMSD ranges, these values indicate marked stability of all four drugs when complexed with M^{pro}. Such complexes can be ranked in terms of stability as follows: lopinavir>atazanavir>birinapant>alpha-mangostin. The low ranking of alpha-mangostin can be explained by the abrupt drift in its RMSD value at 22 nm, observable in Fig. 3. The energy value obtained for alpha-mangostin likewise indicates a lower affinity to M^{pro}. Meanwhile, the per-residue RMSF (Fig. 4) shows conserved RMSF features in M^{pro} complexes with lopinavir, birinapant, and atazanavir. Surprisingly, alpha-mangostin showed several protein fragments with very high RMSD values of 0.4 nm. Nonetheless, based on observations of binding energy, RMSD, and RMSF values, we can exclude alpha-mangostin from being repurposed on the basis of interaction with SARS-CoV-2 M^{pro}.

Radius of gyration

The radius of gyration can be used to determine the compactness of a system, with lower Rg values indicating more stable structures and higher Rg values indicating less compactness or more unfolded protein. All four top drugs had an average Rg value of 2.21 nm; these similar Rg values indicate the stability of the examined drugs when complexed with M^{pro}. Figure 5 shows the variation in Rg obtained during 100 ns MD simulations. Birinapant and ritonavir showed almost similar profiles with less-variable Rg, while alpha-mangostin
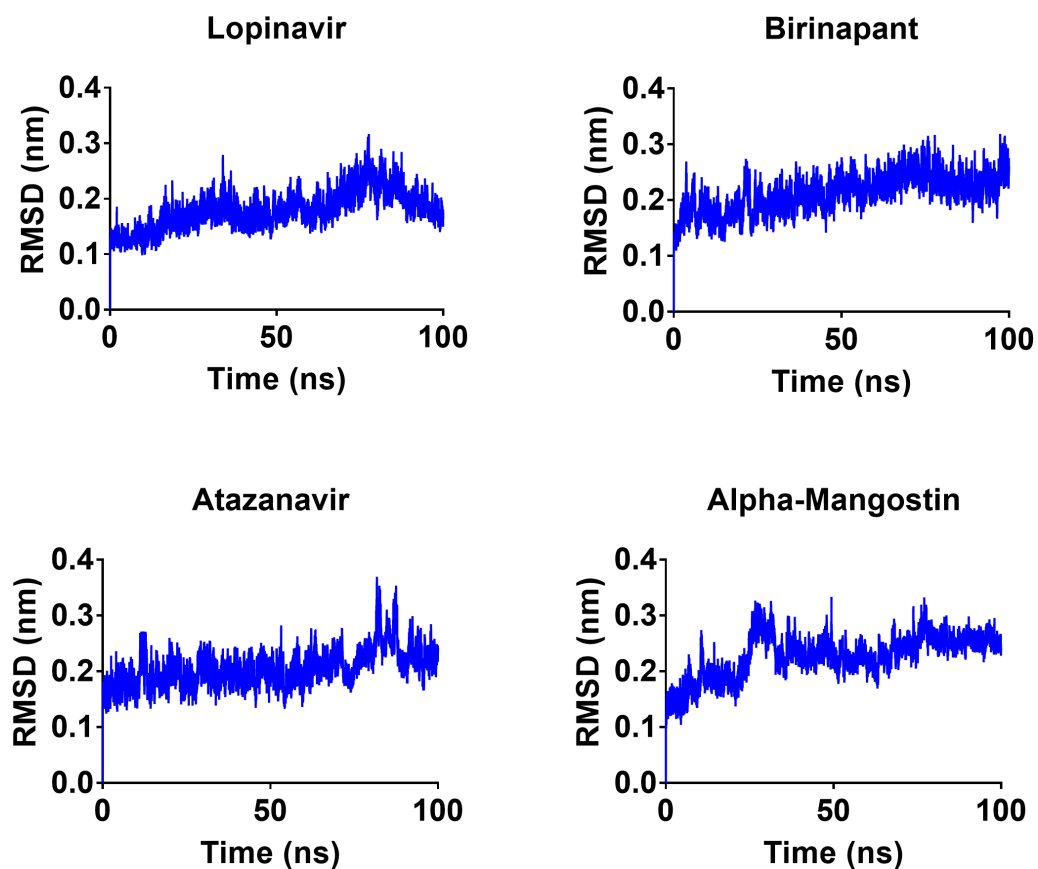
Kandeel et al. (2022), *PeerJ*, DOI 10.7717/peerj.12929

10/20

Lopinavir

Birinapant

Atazanavir

Alpha-Mangostin

Figure 3 RMSD plot of the top four compounds, alpha-mangostin, atazanavir, birinapant and lopinavir, after MDs for 100 ns.

Full-size ⬚ DOI: 10.7717/peerj.12929/fig-3

— Alpha-Mangostin — Atazanavir — Birinapant — Lopinavir
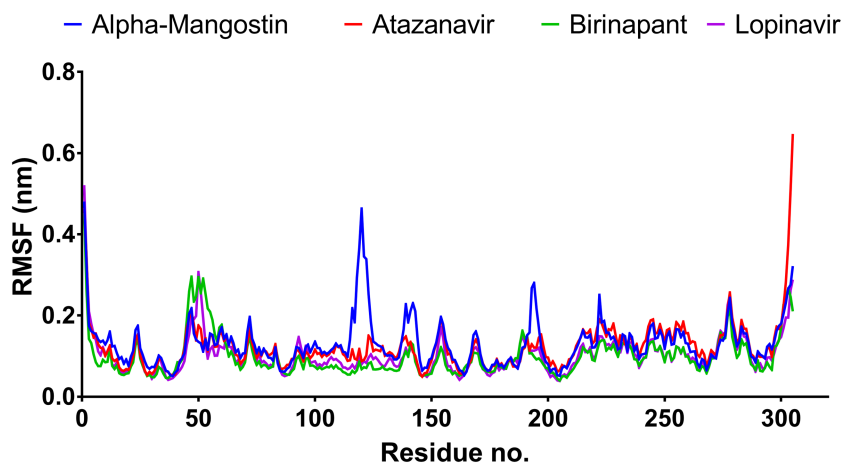
Figure 4 RMSF plot of the top four compounds after MDs for 100 ns.

Full-size ⬚ DOI: 10.7717/peerj.12929/fig-4
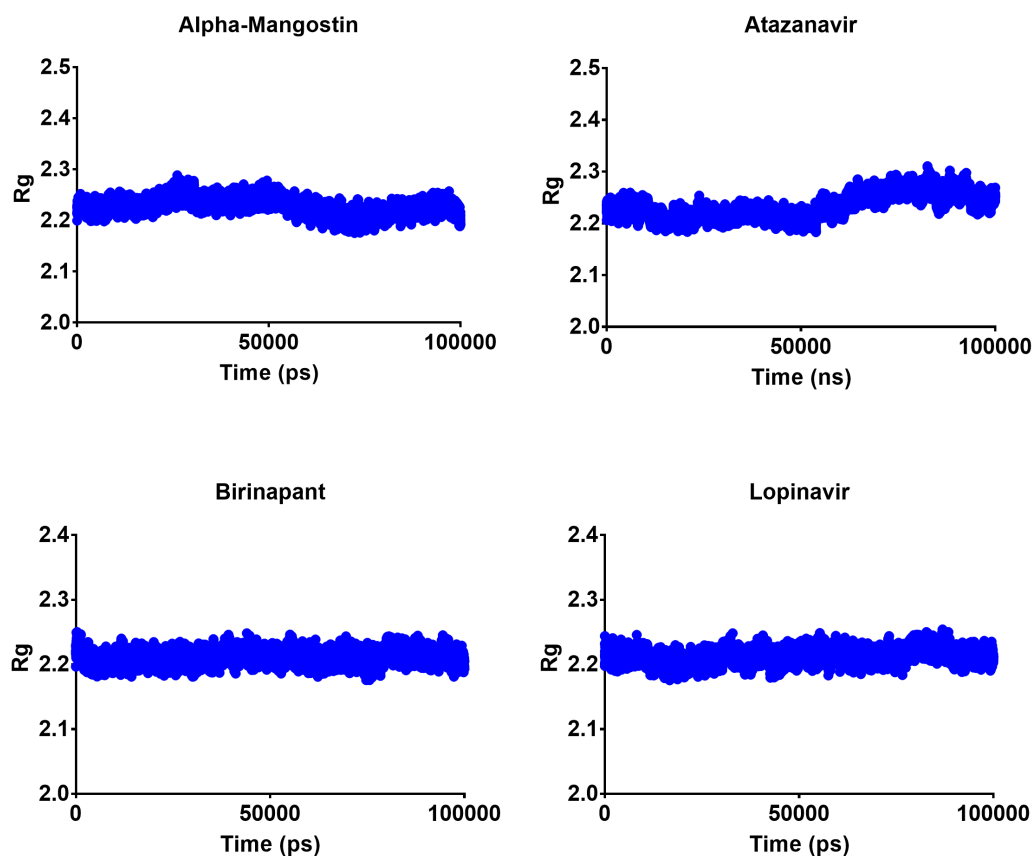
Figure 5 **Radius of gyration of the top four compounds after MDs for 100 ns.**
Full-size 🖼 DOI: 10.7717/peerj.12929/fig-5

and atazanavir showed biphasic profiles of alternating higher and lower Rg. Nonetheless, the overall average Rg values were similar for the four drugs.

Hydrogen bond length

Figure 6 shows the average hydrogen bond length obtained using GLU166 over a 100 ns simulation. Birinapant, with an average length of 0.25 nm, demonstrated the only stable binding with GLU166.

Decomposition of MM-GBSA binding energy

The primary interactions during drug recognition by M^{pro} were studied using post-dynamic energy decomposition analysis (Table 5). The findings revealed that vdw and electrostatic interactions were the most critical forces for all four drugs. More specifically, vdw was the major force for alpha-mangostin, atazanavir, and lopinavir, while electrostatic forces were the major contributor for birinapant binding, with a lesser contribution from vdw.

SARS-CoV-2 Plaque inhibition assay

Plaques inhibition assays in Vero E6 cells were used to explore the drug inhibitory properties against SARS-CoV-2 infection. At a concentration of 10 µM, atazanavir had no antiviral
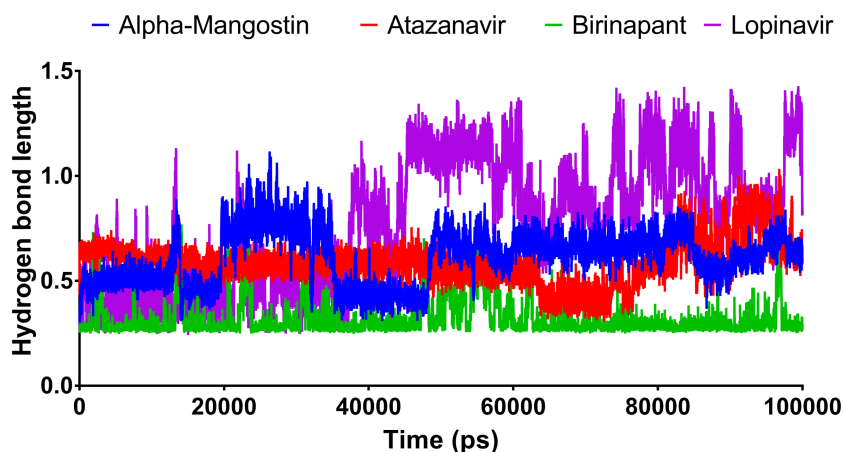
Figure 6 The hydrogen bond length of the top four compounds after MDs for 100 ns.
Full-size ☑ DOI: 10.7717/peerj.12929/fig-6

Table 5 Decomposition of the estimated MMGBSA binding energy for the binding of alpha-mangostin, atazanavir, birinapant and lopinavir with SARS-CoV-2 M^{pro}.

	Alpha-Mangostin	Atazanavir	Birinapant	Lopinavir
van der Waal energy	−184.419	−292.82	−134.625	−227.389
Electrostattic energy	−28.745	−81.919	−305.47	−40.001
Polar solvation energy	113.399	287.534	335.31	177.784
SASA energy	−18.036	−30.595	−16.679	−23.173
Binding energy	−117.863	−117.827	−121.346	−112.801

effects. Birinapant, on the other hand, reduced the production of SARS-CoV-2 plaques by 37% (Fig. 7). Treatment with birinapant significantly inhibited the SARS-CoV-2 plaque formation in a dose-dependent manner. The estimated IC$_{50}$ values for birinapant was 18 ±3.6 µM.

DISCUSSION

With the emergence of SARS-CoV-2 in December 2019 and its rapid worldwide spread, drug repurposing has been one tool available to combat the disease. Many drugs with proven efficiency and safety have been repurposed for other clinical applications. Sildenafil is one such drug; it was initially produced to treat angina and later used for male erectile dysfunction (*Goldstein et al., 1998*); zidovudine was repurposed earlier from an anticancer drug to an anti-HIV agent (*Ashburn & Thor, 2004*), and the antidepressant dapoxetine has been effective in managing premature ejaculation (*Fu, Peng & Hu, 2019*).

The SARS-CoV-2 M^{pro} has been an attractive target in many drug discovery studies. The M^{pro} was targeted by a number of compound libraries, including those containing drugs approved by the Food and Drug Administration (*Kandeel & Al-Nazawi, 2020*), flavonoids and natural compounds (*Joshi et al., 2020*; *Vijayakumar et al., 2020*), tetracycline (*Bharadwaj et al., 2020*) and microbial natural products (*Sayed et al., 2020*). In this study,
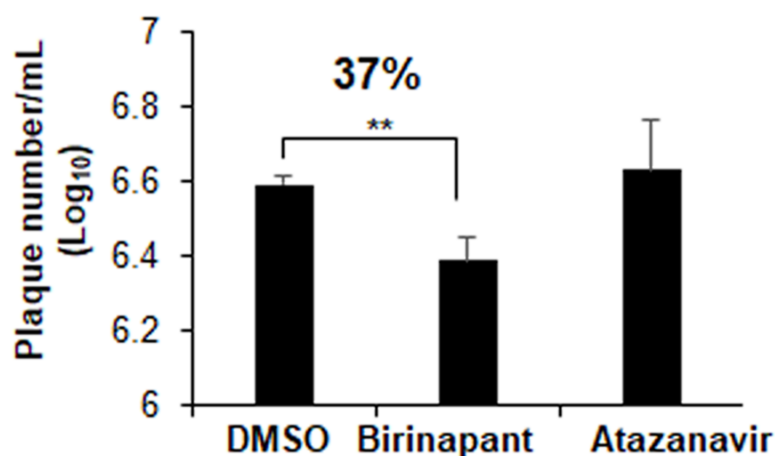
Figure 7 Effect of birinapant and atazanavir on the replication of SARS-CoV-2. Vero E6 cells were infected with 0.1 MOI SARS-CoV-2 in 6-well plate and then treated with DMSO (0.1%), birinapant (10 μM) or atazanavir (10 μM) at 3 h after virus infection ($n = 3$). Supernatants of virus-infected cell cultures were collected at 48 h after virus infection. Virus replication in the supernatants was quantified by plaque formation assay. **$p < 0.01$.

Full-size ⬚ DOI: 10.7717/peerj.12929/fig-7

a large library of virus protein-specific compounds was selected. Initial docking showed interesting docking scores and favourable profiles of structure stability and binding energy. The four drugs selected for the final comprehensive 100 ns MD) simulations were alpha-mangostin, atazanavir, birinapant and lopinavir.

Lopinavir is a well-known protease inhibitor with high efficiency against the HIV-1 protease (*Cvetkovic & Goa, 2003*). In addition, the drug was effective against SARS-CoV and MERS-CoV (*Chan et al., 2015*) and improved the health markers in SARS-CoV-2–infected patients (*Ye et al., 2020*). Atazanavir is another HIV-1 protease inhibitor with the advantage of oral administration in combination with other antiretroviral drugs (*Goldsmith & Perry, 2003*). Birinapant is an apoptosis inhibitor, and it has approved efficiency in controlling viral hepatitis in combination with other antiviral drugs (*Testoni, Durantel & Zoulim, 2017*). Previous *in silico* research showed that birinapant could bind to the main protease of the SARS-CoV-2 virus (*Lokhande et al., 2021*). In our study, in comparison with lopinavir, both atazanavir and birinapant showed an improved XP-docking score, higher binding energy and a lower structural root-mean-square deviation (RMSD) during 100 ns MD simulations. Therefore, based on the clinical efficiency of lopinavir against SARS-CoV-2, the drugs atazanavir and birinapant are expected to perform with similar or improved efficacy comparable to that of ritonavir. Interestingly, it was recently shown that atazanavir can inhibit M^{pro} activity while simultaneously suppressing SARS-CoV-2 replication (*Fintelman-Rodrigues et al., 2020*).

The strong binding profiles of atazanavir and birinapant are supported with hydrophobic interactions. In addition, atazanavir formed two hydrogen bonds with ASN142 and GLU166, and birinapant formed four hydrogen bonds with THR25, GLU166, and GLN192 and a tridentate bond with GLY143, SER144 and CYS145 (Figs. 1E and 1F).

In the second rank, following atazanavir and birinapant, alpha-mangostin and cobicistat showed quite high binding energy but had less structural stability owing to higher RMSD values. Cobicistat is a cytochrome enzyme inhibitor used to increase the systemic availability of other antiviral drugs, such as atazanavir (*Xu et al., 2010*).

After screening investigations, the top two compounds were used in antiviral assays. Atazanavir had no antiviral effects. Atazanavir has been shown to have anti-SARS-CoV-2 action in previous studies (*Fintelman-Rodrigues et al., 2020*). The lack of antiviral effectiveness of atazanavir found in our investigation might indicate that slight differences in the type of virus utilised could alter atazanavir efficacy. In contrast, birinapant has antiviral properties at low micromolar concentrations. The measured EC50 value of birinapant (18 µM) coincides with the measured value for other known antiviral drugs such as remdesivir and lopinavir, which yielded EC50 values against SARS-CoV-2 replication at 23.15 and 26.63 µM, respectively (*Choy et al., 2020*). Birinapant's anti-SARS-CoV-2 activity supports further investigation into its usage as an anti-COVID-19 medication. Combining birinapant with other antivirals may result in considerable SARS-CoV-2 virus particle elimination.

CONCLUSION

After a comprehensive study involving virtual screening, docking, and MD simulations of a unique set of antiviral agents, two highly potent M^{pro}-binding drugs, birinapant and atazanavir, showed promise. These drugs had improved energetic and structural stability profiles that were comparable to or higher than those produced by the classic antiviral protease inhibitor ritonavir. Birinapant was found to inhibit SARS-CoV-2 replication with promising inhibition in the low micromolar range.

ACKNOWLEDGEMENTS

ADDITIONAL INFORMATION AND DECLARATIONS

Competing Interests

The authors declare there are no competing interests.

Author Contributions

- Mahmoud Kandeel conceived and designed the experiments, performed the experiments, analyzed the data, prepared figures and/or tables, authored or reviewed drafts of the paper, and approved the final draft.
- Jinsoo Kim performed the experiments, analyzed the data, prepared figures and/or tables, authored or reviewed drafts of the paper, and approved the final draft.
- Mahmoud Fayez and Yukio Kitade analyzed the data, authored or reviewed drafts of the paper, and approved the final draft.
- Hyung-Joo Kwon conceived and designed the experiments, analyzed the data, authored or reviewed drafts of the paper, and approved the final draft.

Data Availability

The following information was supplied regarding data availability:

The screening results and PDB files are available in the Supplementary Files.

Supplemental Information

Supplemental information for this article can be found online at http://dx.doi.org/10.7717/peerj.12929#supplemental-information.

REFERENCES

Abo Elmaaty A, Hamed MIA, Ismail MI, Eslam BE, Hamada SA, Khattab M, Al-Karmalawy AA. 2021. Computational insights on the potential of some NSAIDs for treating COVID-19: priority set and lead optimization. *Molecules* **26(12)**:3772 DOI 10.3390/molecules26123772.

Abraham MJ, Murtola T, Schulz R, Páll S, Smith JC, Hess B, Lindahl E. 2015. GROMACS: high performance molecular simulations through multi-level parallelism from laptops to supercomputers. *SoftwareX* **1**:19–25.

Al-Hizab F, Kandeel M. 2021. Mycophenolate suppresses inflammation by inhibiting prostaglandin synthases: a study of molecular and experimental drug repurposing. *PeerJ* **9**:e11360 DOI 10.7717/peerj.11360.

Altaher Y, Kandeel M. 2016. Molecular analysis of some camel cytochrome P450 enzymes reveals lower evolution and drug-binding properties. *Journal of Biomolecular Structure and Dynamics* **34**:115–124 DOI 10.1080/07391102.2015.1014423.

Altaher Y, Nakanishi M, Kandeel M. 2015. Annotation of camel genome for estimation of drug binding power, evolution and adaption of cytochrome P450 1a2. *International Journal of Pharmacology* **11**:243–247 DOI 10.3923/ijp.2015.243.247.

Ashburn TT, Thor KB. 2004. Drug repositioning: identifying and developing new uses for existing drugs. *Nature Reviews Drug Discovery* **3**:673–683 DOI 10.1038/nrd1468.

Banerjee S, Yadav S, Banerjee S, Fakayode SO, Parvathareddy J, Reichard W, Surendranathan S, Mahmud F, Whatcott R, Thammathong J, Meibohm B, Miller DD, Jonsson CB, Dubey KD. 2021. Drug repurposing to identify nilotinib as a potential SARS-CoV-2 main protease inhibitor: insights from a computational

Kandeel et al. (2022), *PeerJ*, DOI 10.7717/peerj.12929

16/20

and in vitro study. *Journal of Chemical Information and Modeling* **61**:5469–5483 DOI 10.1021/acs.jcim.1c00524.

Bharadwaj S, Lee KE, Dwivedi VD, Kang SG. 2020. Computational insights into tetracyclines as inhibitors against SARS-CoV-2 M(pro) via combinatorial molecular simulation calculations. *Life Sciences* **257**:118080 DOI 10.1016/j.lfs.2020.118080.

Chan JF-W, Yao Y, Yeung M-L, Deng W, Bao L, Jia L, Li F, Xiao C, Gao H, Yu P. 2015. Treatment with lopinavir/ritonavir or interferon- β1b improves outcome of MERS-CoV infection in a nonhuman primate model of common marmoset. *The Journal of Infectious Diseases* **212**:1904–1913 DOI 10.1093/infdis/jiv392.

Choudhary V, Gupta A, Sharma R, Parmar HS. 2021. Therapeutically effective covalent spike protein inhibitors in treatment of SARS-CoV-2. *Journal of Proteins and Proteomics* **12(4)**:257–270 DOI 10.1007/s42485-021-00074-x.

Choy KT, Wong AY, Kaewpreedee P, Sia SF, Chen D, Hui KPY, Chu DKW, Chan MCW, Cheung PP, Huang X, Peiris M, Yen HL. 2020. Remdesivir, lopinavir, emetine, and homoharringtonine inhibit SARS-CoV-2 replication in vitro. *Antiviral Research* **178**:104786 DOI 10.1016/j.antiviral.2020.104786.

Cucinotta D, Vanelli M. 2020. WHO declares COVID-19 a pandemic. *Acta bio-medica: Atenei Parmensis* **91**:157–160.

Cvetkovic RS, Goa KL. 2003. Lopinavir/ritonavir. *Drugs* **63**:769–802 DOI 10.2165/00003495-200363080-00004.

Delre P, Caporuscio F, Saviano M, Mangiatordi GF. 2020. Repurposing known drugs as covalent and non-covalent inhibitors of the SARS-CoV-2 papain-like protease. *Frontiers in Chemistry* **8**:594009 DOI 10.3389/fchem.2020.594009.

Durdagi S, Orhan MD, Aksoydan B, Calis S, Dogan B, Sahin K, Shahraki A, Iyison NB, Avsar T. 2021. Screening of clinically approved and investigation drugs as potential inhibitors of SARS-CoV-2: a combined in silico and in vitro study. *Molecular Informatics* **40**:2100062 DOI 10.1002/minf.202100062.

Fintelman-Rodrigues N, Sacramento CQ, Ribeiro Lima C, Souzada Silva F, Ferreira AC, Mattos M, de Freitas CS, Cardoso Soares V, da Silva Gomes Dias S, Temerozo JR, Miranda MD, Matos AR, Bozza FA, Carels N, Alves CR, Siqueira MM, Bozza PT, Souza TML. 2020. Atazanavir, alone or in combination with ritonavir, inhibits SARS-CoV-2 replication and proinflammatory cytokine production. *Antimicrobial Agents and Chemotherapy* **64(10)**:e00825–20 DOI 10.1128/aac.00825-20.

Fu M, Peng X, Hu Y. 2019. Effect of premature ejaculation desensitisation therapy combined with dapoxetine hydrochloride on the treatment of primary premature ejaculation. *Andrologia* **51**:e13135 DOI 10.1111/and.13135.

Ghareeb DA, Saleh SR, Nofal MS, Kaddah MMY, Hassan SF, Seif IK, El-Zahaby SA, Khedr SM, Kenawy MY, Masoud AA, Soudi SA, Sobhy AA, Sery JG, El-Wahab MGA, Elmoneam AAA, Al-Mahallawi AM, El-Demellawy MA. 2021. Potential therapeutic and pharmacological strategies for SARS-CoV2. *Journal of Pharmaceutical Investigation* **51**:281–296 DOI 10.1007/s40005-021-00520-4.

Goldsmith DR, Perry CM. 2003. Atazanavir. *Drugs* **63**:1679–1693 DOI 10.2165/00003495-200363160-00003.

Goldstein I, Lue TF, Padma-Nathan H, Rosen RC, Steers WD, Wicker PA. 1998. Oral sildenafil in the treatment of erectile dysfunction. *New England Journal of Medicine* **338**:1397–1404 DOI 10.1056/NEJM199805143382001.

Gurung AB. 2020. In silico structure modelling of SARS-CoV-2 Nsp13 helicase and Nsp14 and repurposing of FDA approved antiviral drugs as dual inhibitors. *Gene Reports* **21**:100860 DOI 10.1016/j.genrep.2020.100860.

Hilgenfeld R. 2014. From SARS to MERS: crystallographic studies on coronaviral proteases enable antiviral drug design. *The FEBS Journal* **281**:4085–4096 DOI 10.1111/febs.12936.

Joshi T, Joshi T, Pundir H, Sharma P, Mathpal S, Chandra S. 2020. Predictive modeling by deep learning, virtual screening and molecular dynamics study of natural compounds against SARS-CoV-2 main protease. *Journal of Biomolecular Structure and Dynamics* **39(17)**:6728–6746 DOI 10.1080/07391102.2020.1802341.

Kandeel M, Abdelrahman AH, Oh-Hashi K, Ibrahim A, Venugopala KN, Morsy MA, Ibrahim MA. 2020. Repurposing of FDA-approved antivirals, antibiotics, anthelmintics, antioxidants, and cell protectives against SARS-CoV-2 papain-like protease. *Journal of Biomolecular Structure and Dynamics* **39(14)**:5129–5136 DOI 10.1080/07391102.2020.1784291.

Kandeel M, Al-Nazawi M. 2020. Virtual screening and repurposing of FDA approved drugs against COVID-19 main protease. *Life Sciences* **251**:117627 DOI 10.1016/j.lfs.2020.117627.

Kandeel M, Altaher A, Alnazawi M. 2019. Molecular dynamics and inhibition of MERS CoV papain-like protease by small molecule imidazole and aminopurine derivatives. *Letters in Drug Design & Discovery* **16**:584–591 DOI 10.2174/1570180815666180918161922.

Kandeel M, Yamamoto M, Park BK, Al-Taher A, Watanabe A, Gohda J, Kawaguchi Y, Oh-Hashi K, Kwon H-J, Inoue J-I. 2021. Discovery of new potent anti-MERS CoV fusion inhibitors. *Frontiers in Pharmacology* **12**:1241 DOI 10.3389/fphar.2021.685161.

Kumari R, Kumar R, Consortium OSDD, Lynn A. 2014. g_mmpbsa? A GROMACS tool for high-throughput MM-PBSA calculations. *Journal of Chemical Information and Modeling* **54**:1951–1962 DOI 10.1021/ci500020m.

Li Y-H, Hu C-Y, Wu N-P, Yao H-P, Li L-J. 2019. Molecular characteristics, functions, and related pathogenicity of MERS-CoV proteins. *Engineering* **5(5)**:940–947 DOI 10.1016/j.eng.2018.11.035.

Lokhande KB, Doiphode S, Vyas R, Swamy KV. 2021. Molecular docking and simulation studies on SARS-CoV-2 M(pro) reveals Mitoxantrone, Leucovorin, Birinapant, and Dynasore as potent drugs against COVID-19. *Journal of Biomolecular Structure and Dynamics* **39**:7294–7305 DOI 10.1080/07391102.2020.1805019.

Mahmoud K, Byoung Kwon P, Mohamed AM, Katharigatta NV, Kentaro O-H, Mohammed A-N, Hyung-Joo K. 2021. Virtual screening and inhibition of middle east respiratory syndrome coronavirus replication by targeting papain-like protease. *Dr Sulaiman Al Habib Medical Journal* **3(4)**:179–187 DOI 10.2991/dsahmj.k.210921.001.

Mandal A, Jha AK, Hazra B. 2021. Plant products as inhibitors of coronavirus 3CL protease. *Frontiers in Pharmacology* **12**:583387–583387 DOI 10.3389/fphar.2021.583387.

Molavi Z, Razi S, Mirmotalebisohi SA, Adibi A, Sameni M, Karami F, Niazi V, Niknam Z, Aliashrafi M, Taheri M, Ghafouri-Fard S, Jeibouei S, Mahdian S, Zali H, Ranjbar MM, Yazdani M. 2021. Identification of FDA approved drugs against SARS-CoV-2 RNA dependent RNA polymerase (RdRp) and 3-chymotrypsin-like protease (3CLpro), drug repurposing approach. *Biomedicine & Pharmacotherapy* **138**:111544 DOI 10.1016/j.biopha.2021.111544.

Mostafa I, Mohamed NH, Mohamed B, Almeer R, Abulmeaty MMA, Bungau SG, El-Shazly AM, Yahya G. 2021. In-silico screening of naturally derived phytochemicals against SARS-CoV main protease. *Environmental Science and Pollution Research* **408**:1–17 DOI 10.1007/s11356-021-17642-9.

Pillaiyar T, Meenakshisundaram S, Manickam M. 2020. Recent discovery and development of inhibitors targeting coronaviruses. *Drug Discovery Today* **25(4)**:668–688 DOI 10.1016/j.drudis.2020.01.015.

Pohl MO, Busnadiego I, Marrafino F, Wiedmer L, Hunziker A, Fernbach S, Glas I, Moroz-Omori EV, Hale BG, Caflisch A, Stertz S. 2021. Combined computational and cellular screening identifies synergistic inhibition of SARS-CoV-2 by lenvatinib and remdesivir. *Journal of General Virology* **102** DOI 10.1099/jgv.0.001625.

Sayed AM, Alhadrami HA, El-Gendy AO, Shamikh YI, Belbahri L, Hassan HM, Abdelmohsen UR, Rateb ME. 2020. Microbial natural products as potential inhibitors of SARS-CoV-2 main protease (M(pro)). *Microorganisms* **8(7)**:970 DOI 10.3390/microorganisms8070970.

Sheikh A, Al-Taher A, Al-Nazawi M, Al-Mubarak AI, Kandeel M. 2020. Analysis of preferred codon usage in the coronavirus N genes and their implications for genome evolution and vaccine design. *Journal of Virological Methods* **277**:113806 DOI 10.1016/j.jviromet.2019.113806.

Testoni B, Durantel D, Zoulim F. 2017. Novel targets for hepatitis B virus therapy. *Liver International* **37**:33–39 DOI 10.1111/liv.13307.

Uddin R, Jalal K, Khan K, Ul-Haq Z. 2021. Re-purposing of hepatitis C virus FDA approved direct acting antivirals as potential SARS-CoV-2 protease inhibitors. *Journal of Molecular Structure* **1250**:131920 DOI 10.1016/j.molstruc.2021.131920.

Uras IS, Ebada SS, Korinek M, Albohy A, Abdulrazik BS, Wang YH, Chen BH, Horng JT, Lin W, Hwang TL, Konuklugil B. 2021. Anti-inflammatory, antiallergic, and COVID-19 main protease (M(pro)) inhibitory activities of butenolides from a marine-derived fungus aspergillus terreus. *Molecules* **26(11)**:3354 DOI 10.3390/molecules26113354.

Van Der Spoel D, Lindahl E, Hess B, Groenhof G, Mark AE, Berendsen HJ. 2005. GROMACS: fast, flexible, and free. *Journal of Computational Chemistry* **26**:1701–1718 DOI 10.1002/jcc.20291.

Vijayakumar BG, Ramesh D, Joji A, Jayachandra Prakasan J, Kannan T. 2020. In silico pharmacokinetic and molecular docking studies of natural flavonoids and synthetic

indole chalcones against essential proteins of SARS-CoV-2. *European Journal of Pharmacology* **886**:173448 DOI 10.1016/j.ejphar.2020.173448.

Xu L, Liu H, Murray BP, Callebaut C, Lee MS, Hong A, Strickley RG, Tsai LK, Stray KM, Wang Y. 2010. Cobicistat (GS-9350): a potent and selective inhibitor of human CYP3A as a novel pharmacoenhancer. *ACS Medicinal Chemistry Letters* **1**:209–213 DOI 10.1021/ml1000257.

Ye X, Luo Y, Xia S, Sun Q, Ding J, Zhou Y, Chen W, Wang X, Zhang W, Du W. 2020. Clinical efficacy of lopinavir/ritonavir in the treatment of Coronavirus disease 2019. *European Review for Medical and Pharmacological Sciences* **24**:3390–3396.

Zaim S, Chong JH, Sankaranarayanan V, Harky A. 2020. COVID-19 and multi-organ response. *Current Problems in Cardiology* **45(8)**:100618 DOI 10.1016/j.cpcardiol.2020.100618.

Zeng Z-Q, Chen D-H, Tan W-P, Qiu S-Y, Xu D, Liang H-X, Chen M-X, Li X, Lin Z-S, Liu W-K. 2018. Epidemiology and clinical characteristics of human coronaviruses OC43, 229E, NL63, and HKU1: a study of hospitalized children with acute respiratory tract infection in Guangzhou, China. *European Journal of Clinical Microbiology & Infectious Diseases* **37**:363–369 DOI 10.1007/s10096-017-3144-z.

Zhang L, Lin D, Kusov Y, Nian Y, Ma Q, Wang J, Brunn Avon, Leyssen P, Lanko K, Neyts J, de Wilde A, Snijder EJ, Liu H, Hilgenfeld R. 2020. α-Ketoamides as broad-spectrum inhibitors of coronavirus and enterovirus replication: structure-based design, synthesis, and activity assessment. *Journal of Medicinal Chemistry* **63**:4562–4578 DOI 10.1021/acs.jmedchem.9b01828.

Zumla A, Chan JF, Azhar EI, Hui DS, Yuen K-Y. 2016. Coronaviruses—drug discovery and therapeutic options. *Nature Reviews Drug discovery* **15**:327 DOI 10.1038/nrd.2015.37.